

Dielectric properties and crystallite size distribution of modified lead-free sodium-bismuth titanate ceramics

E. D. Politova, G. M. Kaleva, S. A. Ivanov, A. V. Mosunov, S. Yu. Stefanovich, N. V. Sadovskaya & V. V. Shvartsman

To cite this article: E. D. Politova, G. M. Kaleva, S. A. Ivanov, A. V. Mosunov, S. Yu. Stefanovich, N. V. Sadovskaya & V. V. Shvartsman (2023) Dielectric properties and crystallite size distribution of modified lead-free sodium-bismuth titanate ceramics, *Ferroelectrics*, 605:1, 73-82, DOI: [10.1080/00150193.2023.2169012](https://doi.org/10.1080/00150193.2023.2169012)

To link to this article: <https://doi.org/10.1080/00150193.2023.2169012>



Published online: 15 Mar 2023.



Submit your article to this journal [↗](#)



View related articles [↗](#)



View Crossmark data [↗](#)



Dielectric properties and crystallite size distribution of modified lead-free sodium-bismuth titanate ceramics

E. D. Politova^a , G. M. Kaleva^a, S. A. Ivanov^{a,b}, A. V. Mosunov^b, S. Yu. Stefanovich^b, N. V. Sadovskaya^c, and V. V. Shvartsman^d

^aN. N. Semenov Federal Research Center for Chemical Physics, Russian Academy of Sciences, Moscow, Russia; ^bFaculty of Chemistry, Lomonosov Moscow State University, Moscow, Russia; ^cInstitute of Crystallography, Federal Research Center “Crystallography and Photonics, Russian Academy of Sciences, Moscow, Russia; ^dInstitute for Materials Science, University of Duisburg-Essen, Essen, Germany

ABSTRACT

Influence of $(\text{K}_{0.5}\text{Bi}_{0.5})\text{TiO}_3$ (KBT) dopants on crystal and microstructure, ferroelectric and dielectric properties of ceramic composition from morphotropic phase boundary in the system $(1-x-y)$ $(\text{Na}_{0.5}\text{Bi}_{0.5})\text{TiO}_3 - x\text{BaTiO}_3 - y(\text{K}_{0.5}\text{Bi}_{0.5})\text{TiO}_3$ ($x = 0.06$, $y = 0-0.15$) additionally modified by ZnO additives was studied using a complex of methods. Changes from 42.8 nm to 62.6 nm of the volume-weighted crystallite size distribution function $G(L)$ corresponding to coherent scattering regions were observed. The microstructure and the second harmonic generation data indicated a change in the relative content of polar nanoregions in tetragonal nonpolar matrix. Decrease in temperatures of phase transitions T_m and T_d was observed with KBT concentration increasing.

ARTICLE HISTORY

Received 24 August 2022
Accepted 12 January 2023

KEYWORDS

Sodium-potassium niobate; perovskite structure; crystallite size; dielectric properties

1. Introduction

During the last years, Pb-free oxides were intensively studied to replace piezoelectric materials containing environmentally dangerous toxic lead oxide [1–9]. However, despite numerous studies, development of new Pb-free materials with properties compared to those of lead zirconium-titanate-based oxides still remains a task to be solved [10].

Sodium-bismuth titanate (NBT) based perovskite relaxor ferroelectric oxides comprise especially promising ones for the development of new lead-free materials with enhanced piezoelectric, energy storage, electrocaloric, and other properties [11–16]. A lot of work, was devoted to the study of the influence of various acceptor and donor dopants in A- and B-sites of perovskite lattice on the changes in the functional properties of materials [17–22].

The compositions from morphotropic phase boundaries (MPB) in the $(\text{Na}_{0.5}\text{Bi}_{0.5})\text{TiO}_3 - \text{BaTiO}_3$ (NBT-BT) and $(\text{Na}_{0.5}\text{Bi}_{0.5})\text{TiO}_3 - \text{BaTiO}_3 - (\text{K}_{0.5}\text{Bi}_{0.5})\text{TiO}_3$ (NBT-BT-KBT) systems are among the most intensively studied [23–29]. However, the results obtained are poorly consistent. This may be explained by difficulties in the preparation of stoichiometric compositions with reproducible properties related to poorly controlled losses of highly volatile bismuth and sodium oxides during sintering. It is

also known that A-site cation deficiency and Na/Bi ratio influence structural parameters and functional properties of NBT-based ceramics [30–32].

In this work, the influence of tetragonal antiferroelectric $(\text{K}_{0.5}\text{Bi}_{0.5})\text{TiO}_3$ (KBT) on structure parameters, microstructure, and dielectric properties of compositions close to the MPB in the system NBT-BT-KBT additionally modified by ZnO additive has been studied.

2. Experimental

Ceramic samples $(1-x-y)(\text{Na}_{0.5}\text{Bi}_{0.5})\text{TiO}_3 - x\text{BaTiO}_3 - y(\text{K}_{0.5}\text{Bi}_{0.5})\text{TiO}_3$ (NBT-BT-KBT) with $x = 0.06$, $y = 0.0, 0.025, 0.05, 0.10, 0.15$ were prepared by the solid-state reaction method at calcinations temperatures of $T_1 = 1073$ K (6 h), and sintering temperatures of $T_2 = 1373$ K and 1423 K (3 h). The samples were additionally modified by 1.5 w.% of ZnO additives in order to improve the properties of ceramics.

Sodium carbonate Na_2CO_3 , barium carbonate BaCO_3 , potassium carbonate K_2CO_3 , Bi_2O_3 , TiO_2 , and ZnO oxides (all “pure” grade) were used as starting materials. Carbonates were dried at 673 K before synthesis in order to remove absorbed water.

Phase content, structure parameters, and microstructure of the samples were characterized using X-ray diffraction (XRD, DRON-3M, Cu-K_α radiation, 2θ range of $5 \div 80$ degrees with steps 0.05 and 0.02 grad.), and scanning electron microscopy (SEM, JEOL YSM-7401F with the JED-2300 energy dispersive X-ray spectrometer system) methods. Dielectric measurements were performed using ceramics with fired silver electrodes on heating and cooling with 10 K/min. in the temperature interval of $300 \div 1000$ K and the frequency range of 100 Hz \div 1 MHz using Agilent 4284 A (1 V). The second harmonic generation (SHG) method was used to check spontaneous polarization value of the samples using the Nd:YAG laser, $\lambda = 1.064$ μm , in the reflection mode.

Since the X-ray diffraction method is sensitive to the size of coherent scattering blocks, a thorough analysis of powder diffraction data may be used to describe the fine structure of the studied ceramics. In this paper, their average sizes are characterized using a volume-weighted crystallite size distribution function $G(L)$ [31,32], which can be interpreted as the probability density of finding a crystallite of the assumed size in the analyzed sample taken with a weight proportional to its volume. Diffraction patterns were measured on an automatic powder diffractometer DRON-3M using Cu-K_α radiation. Reflections were measured by step-by-step scanning with variable steps (depending on the intensity of reflections) for all the tested samples. The experimental intensities were adjusted taking into account the Lorentz polarization coefficient, and the background was removed with an assumed linear change. Corrections for instrumental and spectral expansion were made using the corundum standard (NIST). Pure diffraction lines were obtained using the Luer–Weigel–Louboutin (LWL) deconvolution method [31,32]. The method was implemented in the PROFIT profile analysis computer program [33]. From the comparison of the measured intensity data for the sample and the standard, the corresponding correct profile of the line $f(x)$ was extracted using the pseudo-Voigt function. The size distribution functions $G(L)$ were determined from $f(x)$, following the procedure proposed in refs. [31,32] and described in detail in refs. [33,34].

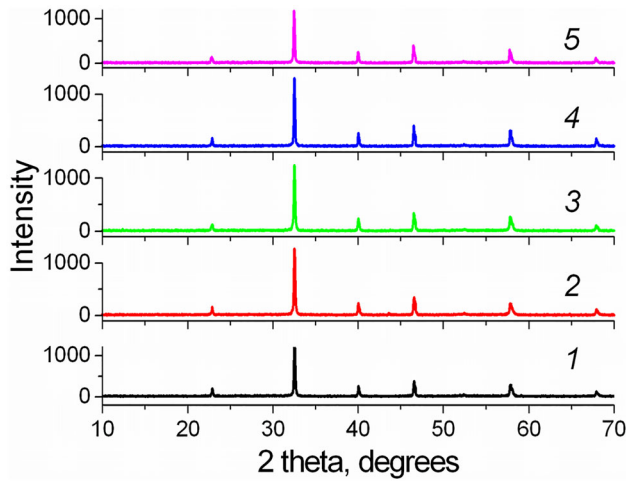


Figure 1. X-ray diffraction patterns of the samples $(1-x-y)(\text{Na}_{0.5}\text{Bi}_{0.5})\text{TiO}_3 - x\text{BaTiO}_3 - y(\text{K}_{0.5}\text{Bi}_{0.5})\text{TiO}_3$ with $x=0.06$, $y=0.0$ (1), 0.025 (2), 0.05 (3), 0.10 (4), 0.15 (5) prepared at sintering temperature of $T_2 = 1373$ K (3 h).

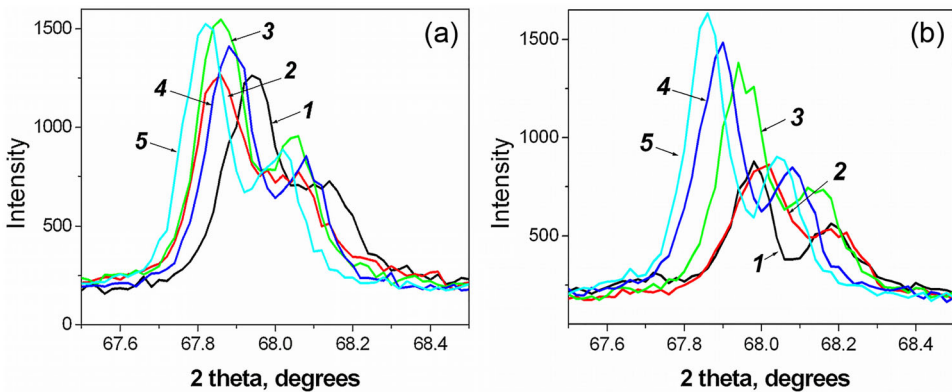


Figure 2. (a) Fragments of X-ray diffraction patterns of the samples $(1-x-y)(\text{Na}_{0.5}\text{Bi}_{0.5})\text{TiO}_3 - x\text{BaTiO}_3 - y(\text{K}_{0.5}\text{Bi}_{0.5})\text{TiO}_3$ with $x=0.06$, $y=0.0$ (1), 0.025 (2), 0.05 (3), 0.10 (4), 0.15 (5) prepared at sintering temperature of $T_2 = 1373$ K (3 h) and (b) of the samples modified by ZnO prepared at $T_2 = 1423$ K (4 h).

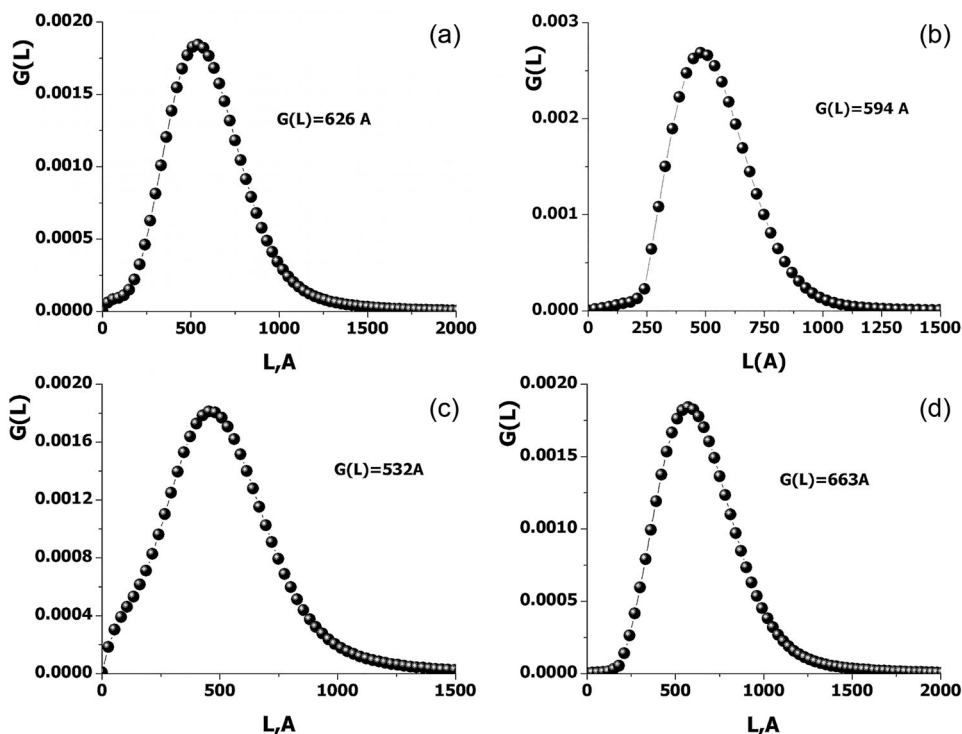
3. Results and discussion

Pure NBT-BT-KBT samples with perovskite structure were obtained for all the compositions studied (Fig. 1). The samples studied are characterized by pseudocubic structure (Fig. 2). As it is seen in Figure 2(a, b), an increase in amount of the KBT additives leads to a shift of the diffraction peaks to lower angles and to a corresponding increase in the pseudocubic unit cell volume from 59.19 to 59.47 \AA^3 (Table 1) in accordance with larger K^+ ionic radius. The ZnO containing samples have a bit lower unit cell volume that indicates introduction of Zn^{2+} ions into A-positions of perovskite lattice.

In order to estimate the distribution of crystallites by the size of the ceramic samples prepared, an analysis of the XRD data line profile for the selected peaks was performed. The tested samples contained convenient single reflections of higher orders of

Table 1. The unit cell parameters of the NBT-BT-KBT samples obtained by Profit program.

	$\langle a \rangle$ (Å)	V (Å ³)	$G(L)$	T_2 (K)
Samples NBT-BT-KBT				
$x = 0.06, y = 0$	3.8978 (2)	59.22	536	1373
$x = 0.06, y = 0$	3.8972 (2)	59.19	626	1423
$x = 0.06, y = 0.15$	3.9027 (2)	59.44	579	1373
$x = 0.06, y = 0.15$	3.9033 (2)	59.47	594	1423
Samples NBT-BT-KBT + ZnO				
$x = 0.06, y = 0$	3.8926 (2)	58.98	532	1423
$x = 0.06, y = 0.15$	3.9002 (2)	59.33	663	1423

**Figure 3.** The volume-weighted crystallite size distribution $G(L)$ for (a, b) NBT-BT-KBT samples (c, d) modified by ZnO with (a, c) $y = 0$ and (b, d) $y = 0.15$ sintered at 1423 K (3 h).

diffraction from the same set of crystal planes; therefore, it seemed possible to separate the contribution to the expansion of the lines from the influence of the dimensional effect and distortions associated with microstresses.

By checking the average shape of the crystallites based on the analysis of several lines, it was found that the observed broadening of the diffraction lines was most likely due to dimensional effects. The volume-weighted functions of the crystallite size distribution $G(L)$ along the crystallographic direction (110) are shown in Figure 3. A characteristic feature of all the size distributions obtained is their unimodality. In most cases, this distribution may be explained by a similar mechanism of particle formation in the process of solid-phase synthesis.

The $G(L)$ value increases for samples with $y = 0.15$ in comparison to that for the samples with $y = 0$ corresponding to data presented in Figure 2. Introduction of K^+ ions

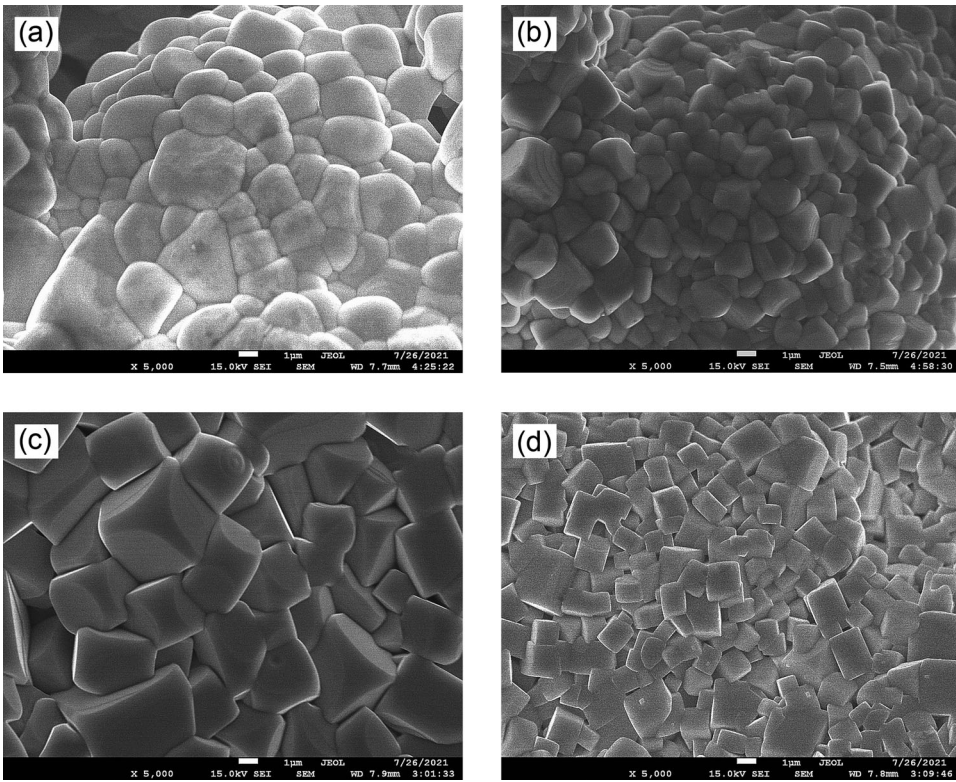


Figure 4. Microstructure of the NBT-BT-KBT samples with $x = 0.06$, (a) $y = 0.025$, (b) $y = 0.15$; and ZnO modified samples with (c) $y = 0.05$, (d) $y = 0.15$. Bars – 1 μm .

leads to an increase in the $G(L)$ value parameter. Increase in the $G(L)$ values is observed in all the samples sintered at higher temperatures as well. These effects may be explained by the specific mechanism of particle formation.

Nonuniform distribution of A-cations in the samples with $x = 0.06$ and $y = 0 \div 0.15$ may explain the changes in the relative content of polar nanometer-size ferroelectric rhombohedral clusters in non-polar tetragonal matrix typical of the NBT-based samples [19,35].

Microstructure of the samples correlates with the structure of the samples and is sensitive to substitutions and sintering conditions (Fig. 4). Introduction of KBT leads only to a slight decrease in the average size of the grains with y increasing. In the case of ZnO modified samples, this decrease is more pronounced. Moreover, with increasing y value the grains become more rectangular in form corresponding to the increasing relative content of nonpolar tetragonal matrix.

For the NBT-BT-KBT samples, maxima at $\sim 550 \div 600$ K were revealed in the dielectric permittivity versus temperature curves (Fig. 5). Besides, strongly diffused steps were revealed near $300 \div 400$ K indicating a transition from antiferroelectric to ferroelectric phase. They reveal typical relaxor-type behavior confirming the presence of polar nano-regions in a nonpolar matrix. Moreover, at temperatures near 800 K relaxor peaks were also observed in the samples with increased total conductivity at high temperatures confirming the presence of oxygen vacancies in the lattice. It should be noted that high

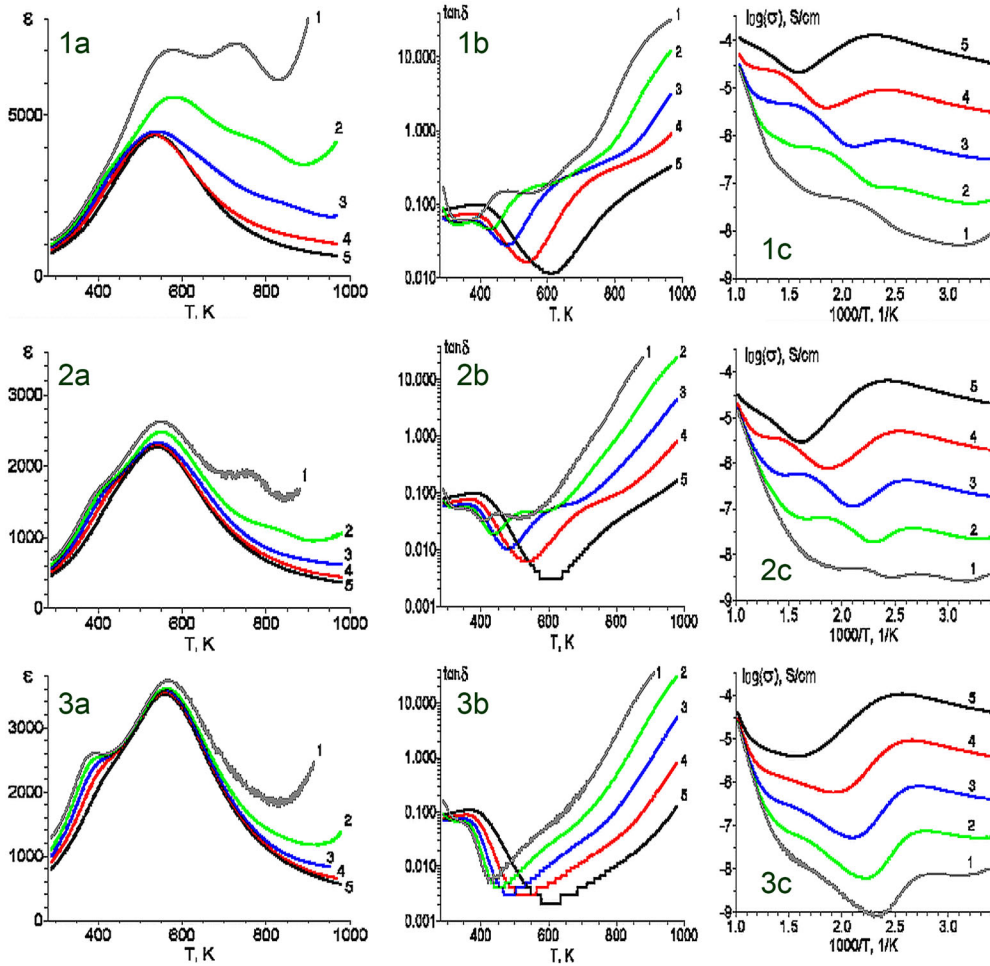


Figure 5. Temperature dependences of (a) dielectric permittivity $\varepsilon(T)$, (b) dielectric loss $\tan\delta(T)$ and (c) electroconductivity $\log(\sigma)(1/T)$ of the samples with $y=0.0$ (1a–c), 0.025 (2a–c), 0.05 (3a–c), 0.15 (4a–c) sintered at 1423 K measured at frequencies $f=100$ Hz (1), 1 kHz (2), 10 kHz (3), 100 kHz (4), 1 MHz (5).

conductivity at high temperatures is obviously connected to the formation of oxygen vacancies in the samples with A-sites deficiency [24,31–35]. Moreover, high total conductivity at high temperatures 1000 K in compositions with $y=0$ (Fig. 6) and in ZnO-modified samples with $y=0$ and 0.025 (Fig. 6) confirmed presence of oxygen vacancies in these samples.

A slight decrease in the temperatures of both phase transitions T_m and T_d was observed in ceramic solid solutions (Fig. 7a). It is important that dielectric permittivity at the room temperature increased in doped samples with the highest values in the samples with $x=0.10$.

At the room temperature, intensity of the SHG signal q is higher than q value for standard SiO_2 powder that confirmed a noncentrosymmetric structure of the NBT-based oxides and their ferroelectric properties (Fig. 7b). It should be noted that in initial NBT oxide q values are practically two orders lower than those measured for typical ferroelectrics BaTiO_3 and $(\text{K}, \text{Na})\text{NbO}_3$ having close values of spontaneous polarization $P_s \sim$

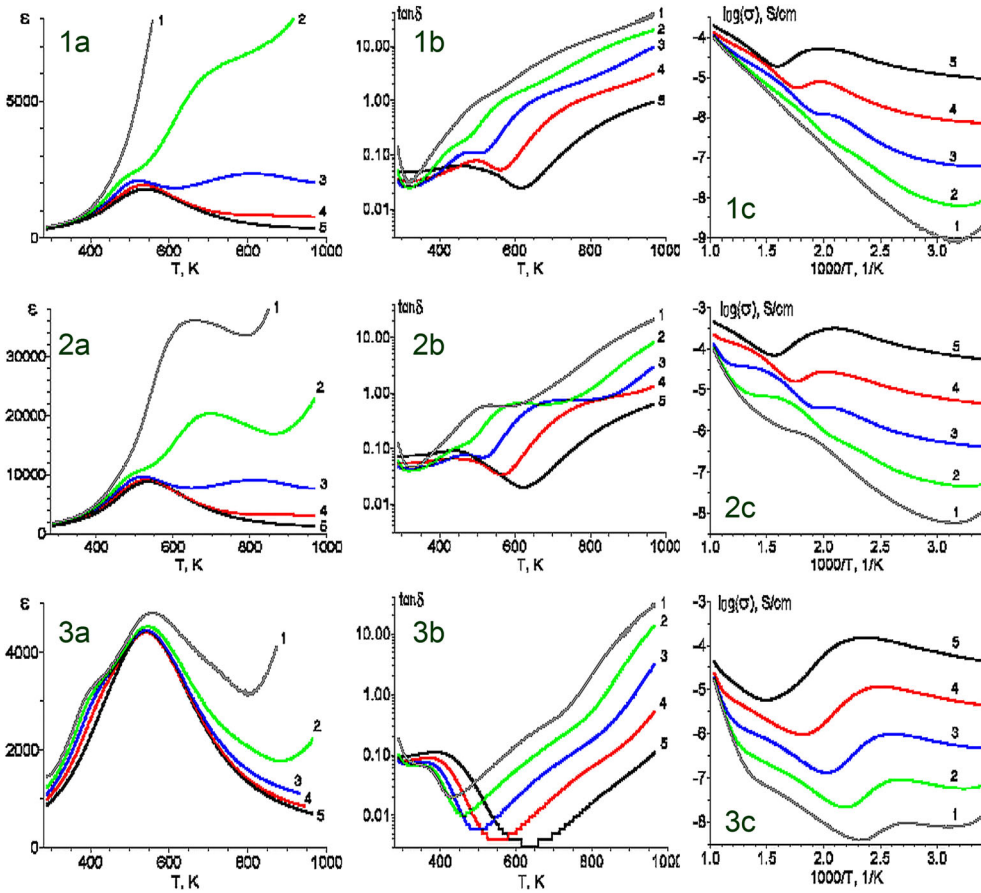


Figure 6. Temperature dependences of (a) dielectric permittivity $\epsilon(T)$, (b) dielectric loss $\tan\delta(T)$ and (c) electroconductivity $\lg\sigma(1/T)$ of the ZnO modified samples with $y=0.0$ (1a–c), 0.025 (2a–c), 0.15 (3a–c) sintered at 1423 K measured at frequencies $f=100$ Hz (1), 1 kHz (2), 10 kHz (3), 100 kHz (4), and 1 MHz (5).

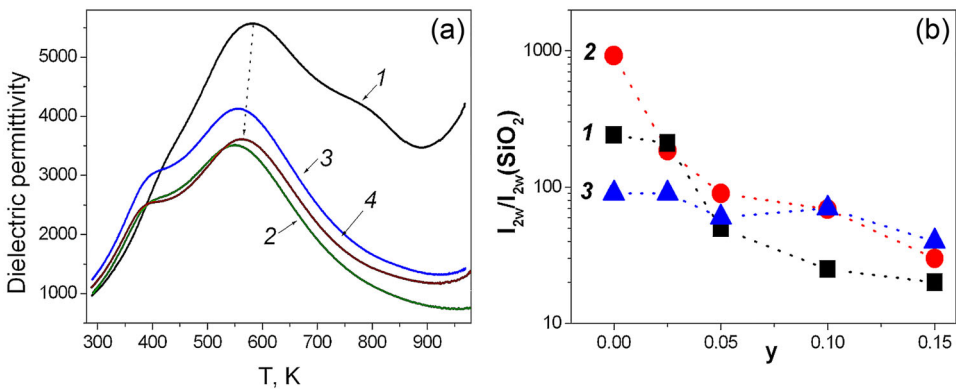


Figure 7. (a) Temperature dependences of dielectric permittivity $\epsilon(T)$ of the samples with $x=0.06$, $y=0$ (1), 0.05 (2), 0.10 (3), 0.15 (4), prepared at $T_2 = 1273$ K (3 h) measured at frequency $f=1$ kHz. (b) Concentration dependences of the SHG signal of the NBT-BT-KBT samples (1) and modified by ZnO (2, 3) sintered at $T_2 = 1373$ K (2) and 1423 K (1, 3).

$25 \div 38 \mu\text{C}/\text{cm}^2$ [29,30]. This is a result of specific nature of relaxor NBT oxide described as a presence of polar nanometer-size ferroelectric rhombohedral clusters in non-polar tetragonal matrix. Formation of such polar nanoregions was explained by the presence of accidental electric fields determined by randomly distributed A-cations in the perovskite lattice [19,35].

The results obtained confirm that electrical properties of NBT-based compositions are highly sensitive to the A-site substitutions and clearly show that dielectric permittivity values depend on initial reagents, additives, and sintering temperatures. A decrease in both SHG signal value and ferroelectric-to-relaxor transition temperature indicates that the long-range ferroelectric order is destroyed in compositions with $y \geq 0.05$ [36].

The observed behavior is also consistent with the results of the volume-weighted crystallite size distribution function $G(L)$ and microstructure data indicating real changes in relative content of polar nanoregions and tetragonal nonpolar matrix.

4. Conclusion

Structure parameters, microstructure, dielectric, and ferroelectric properties of the $(1-x-y)$ $(\text{Na}_{0.5}\text{Bi}_{0.5})\text{TiO}_3 - x\text{BaTiO}_3 - y(\text{K}_{0.5}\text{Bi}_{0.5})\text{TiO}_3$ solid solutions and additionally modified by the ZnO overstoichiometric additives were studied. Influence of dopants and sintering conditions on the unit cell parameters, volume-weighted crystallite size distribution $G(L)$, and temperatures of phase transitions was observed. The volume-weighted crystallite size distribution $G(L)$ values changed from 42.8 nm till 62.6 nm depending on solid solutions compositions and sintering conditions. A decrease in temperatures of phase transitions T_m and T_d was observed with KBT concentration increasing.

Funding

The work was supported by RFBR and DFG (project number 21-53-12005) and by the Ministry of Science and Higher Education of the Russian Federation for the Russian Academy of Sciences (No. 45.22 AAAA-A18-118012390045-2), and within the state assignment FSRC “Crystallography and Photonics” RAS.

ORCID

E. D. Politova  <http://orcid.org/0000-0002-4158-6314>

References

- [1] S. J. Zhang, R. Xia, and R. T. ShROUT, Lead-free piezoelectric ceramics: Alternatives for PZT?, *J. Electroceram.* **19** (4), 251 (2007). DOI: [10.1007/s10832-007-9047-0](https://doi.org/10.1007/s10832-007-9047-0).
- [2] T. Takenaka, H. Nagata, and Y. Hiruma, Current developments and prospective of lead-free piezoelectric ceramics, *Jpn. J. Appl. Phys.* **47** (5), 3787 (2008). DOI: [10.1143/JJAP.47.3787](https://doi.org/10.1143/JJAP.47.3787).
- [3] D. Damjanovic *et al.*, What can be expected from lead-free piezoelectric materials?, *Funct. Mater. Lett.* **3**, 5–13 (2010). DOI: [10.1142/S1793604710000919](https://doi.org/10.1142/S1793604710000919).
- [4] D. Xiao, Progresses and further considerations on the research of perovskite lead-free piezoelectric ceramics, *J. Adv. Dielect.* **1**, 33–40 (2011). DOI: [10.1142/S2010135X11000045](https://doi.org/10.1142/S2010135X11000045).

- [5] I. Coondoo, N. Panwar, and A. Kholkin, Lead-free piezoelectrics: Current status and perspective, *J. Adv. Dielect.* **03** (02), 1330002 (2013). DOI: [10.1142/S2010135X13300028](https://doi.org/10.1142/S2010135X13300028).
- [6] P. Panda, and B. Sahoo, PZT to lead-free piezoceramics: A review, *Ferroelectrics* **474** (1), 128 (2015). DOI: [10.1080/00150193.2015.997146](https://doi.org/10.1080/00150193.2015.997146).
- [7] C. H. Hong *et al.*, Lead-free piezoceramics. Where to move on? *J. Materiomics* **2**, 1 (2016). DOI: [10.1016/j.jmat.2015.12.002](https://doi.org/10.1016/j.jmat.2015.12.002).
- [8] J. Rodel, and J. Li, Lead-free piezoceramics: Status and perspectives, *MRS Bull.* **43** (8), 576 (2018). DOI: [10.1557/mrs.2018.181](https://doi.org/10.1557/mrs.2018.181).
- [9] X. Zhou *et al.*, Phase structure and properties of sodium bismuth titanate lead-free piezoelectric ceramics, *Prog. Mat. Sci.* **122**, 100836 (2021). DOI: [10.1016/j.pmatsci.2021.100836](https://doi.org/10.1016/j.pmatsci.2021.100836).
- [10] J. Koruza, L. K. Venkataraman, and B. Malic, Lead-free perovskite ferroelectrics, in *Magnetic, Ferroelectric, and Multiferroic Metal Oxides*, Ed. B. D. Stojanovic, pp. 41–69. (Elsevier, 2018). DOI: [10.1016/B978-0-12-811180-2.00003-7](https://doi.org/10.1016/B978-0-12-811180-2.00003-7).
- [11] G. A. Smolenskii *et al.*, New ferroelectrics of complex composition, *Fiz. Tverd. Tela* **2**, 2651 (1961). Corpus ID: 210517302.
- [12] S. B. Vakhrushev *et al.*, Phase transitions and soft modes in sodium bismuth titanate, *Ferroelectrics* **63** (1), 153 (1985). DOI: [10.1080/00150198508221396](https://doi.org/10.1080/00150198508221396).
- [13] K. Reichmann, A. Feteira, and M. Li, Bismuth sodium titanate based materials for piezoelectric actuators, *Materials (Basel)* **8** (12), 8467 (2015). DOI: [10.3390/ma8125469](https://doi.org/10.3390/ma8125469).
- [14] V. J. Vodyanoy, and Y. Mnyukh, The physical nature of “giant” magnetocaloric and electrocaloric effects, *Am. J. Mat. Sci.* **3**, 105 (2013). DOI: [10.5923/j.materials.20130305.01](https://doi.org/10.5923/j.materials.20130305.01).
- [15] F. Weyland *et al.*, Critically: Concept to Enhance the piezoelectric and electrocaloric properties of ferroelectrics, *Adv. Funct. Mater.* **26** (40), 7326 (2016). DOI: [10.1002/adfm.201602368](https://doi.org/10.1002/adfm.201602368).
- [16] A. Kumar *et al.*, Prospects and challenges of the electrocaloric phenomenon in ferroelectric ceramics, *J. Mater. Chem. C* **7**, 6836 (2019). DOI: [10.1039/C9TC01525F](https://doi.org/10.1039/C9TC01525F).
- [17] Y. Hiruma, H. Nagata, and T. Takenaka, Phase diagrams and electrical properties of $(\text{Bi}_{1/2}\text{Na}_{1/2})\text{TiO}_3$ -based solid solutions, *J. Appl. Phys.* **104** (12), 124106 (2008). DOI: [10.1063/1.3043588](https://doi.org/10.1063/1.3043588). [Database].
- [18] B. Parija *et al.*, Ferroelectric and piezoelectric properties of $(1-x)(\text{Bi}_{0.5}\text{Na}_{0.5})\text{TiO}_3 - x\text{BaTiO}_3$ ceramics, *J. Mater. Sci.: Mater. Electron* **24**, 402 (2013). DOI: [10.1007/s10854-012-0764-z](https://doi.org/10.1007/s10854-012-0764-z).
- [19] Y. S. Sung, and M. H. Kim, Effects of B-site donor and acceptor doping in Pb-free $(\text{Bi}_{0.5}\text{Na}_{0.5})\text{TiO}_3$ ceramics, in *Technical Ferroelectrics*, edited by I. Coondoo (INTECH, Croatia, 2010), pp. 217–230. DOI: [10.5772/13903](https://doi.org/10.5772/13903).
- [20] V. V. Shvartsman, and D. C. Lupascu, Lead-free relaxor ferroelectrics, *J. Am. Ceram. Soc.* **95**, 1 (2012). DOI: [10.1111/J.1551-2916.2011.04952.X](https://doi.org/10.1111/J.1551-2916.2011.04952.X).
- [21] A. R. Paterson *et al.*, Relaxor-ferroelectric transitions: Sodium bismuth titanate derivatives, *MRS Bull.* **43** (8), 600 (2018). DOI: [10.1557/mrs.2018.156](https://doi.org/10.1557/mrs.2018.156).
- [22] M. Li *et al.*, The dramatic influence of A-site non-stoichiometry on the electrical conductivity and conduction mechanisms in the perovskite oxide $\text{Na}_{0.5}\text{Bi}_{0.5}\text{TiO}_3$, *Chem. Mater.* **27** (2), 629 (2015). DOI: [10.1021/cm504475k](https://doi.org/10.1021/cm504475k).
- [23] I.-T. Seo, S. Steiner, and T. Frömling, The effect of A site non-stoichiometry on $0.94(\text{Na}_y\text{Bi}_x)\text{TiO}_3-0.06\text{BaTiO}_3$, *J. Eur. Cer. Soc.* **37** (4), 1429 (2017). DOI: [10.1016/j.jeurceramsoc.2016.11.045](https://doi.org/10.1016/j.jeurceramsoc.2016.11.045).
- [24] M. Mesrar *et al.*, Effect of barium doping on electrical and electromechanical properties of $(1-x)(\text{Na}_{0.5}\text{Bi}_{0.5})\text{TiO}_3-x\text{BaTiO}_3$, *Mediterr. J.Chem.* **8** (3), 198 (2019). DOI: [10.13171/10.13171/mjc8319050908mm](https://doi.org/10.13171/10.13171/mjc8319050908mm).
- [25] W. Chen *et al.*, Electromechanical properties and morphotropic phase boundary of $\text{Na}_{0.5}\text{Bi}_{0.5}\text{TiO}_3-\text{K}_{0.5}\text{Bi}_{0.5}\text{TiO}_3-\text{BaTiO}_3$ lead-free piezoelectric ceramics, *J. Electroceram.* **15** (3), 229 (2005). DOI: [10.1007/s10832-005-3301-0](https://doi.org/10.1007/s10832-005-3301-0).
- [26] Y. Hiruma, H. Nagata, and T. Takenaka, Phase transition temperatures and piezoelectric properties of $(\text{Bi}_{1/2}\text{Na}_{1/2})\text{TiO}_3-(\text{Bi}_{1/2}\text{K}_{1/2})\text{TiO}_3-\text{BaTiO}_3$ lead-free piezoelectric ceramics, *Jpn. J. Appl. Phys.* **45** (9B), 7409 (2006). DOI: [10.1143/JJAP.45.7409](https://doi.org/10.1143/JJAP.45.7409).

- [27] Y. Li *et al.*, Phase structure and electrical properties of lead-free (1-2x)NBT-xKBT-xBT ceramics, *J. Mater. Sci: Mater. Electron.* **29** (9), 7851 (2018). DOI: [10.1007/s10854-018-8784-y](https://doi.org/10.1007/s10854-018-8784-y).
- [28] E. D. Politova *et al.*, Phase transitions, ferroelectric and relaxor properties of nonstoichiometric NBT ceramics, *Ferroelectrics* **538** (1), 120 (2019). DOI: [10.1080/00150193.2019.1569994](https://doi.org/10.1080/00150193.2019.1569994).
- [29] E. D. Politova *et al.*, Specific features of the structure and the dielectric properties of sodium-bismuth titanate-based ceramics, *Phys. Solid State* **60** (3), 428 (2018). DOI: [10.1134/S1063783418030265](https://doi.org/10.1134/S1063783418030265).
- [30] E. D. Politova *et al.*, Physics and chemistry of creating new titanates with perovskite structure, *Russ. J. Phys. Chem. A* **92**, 1132 (2018). DOI: [10.1134/S0036024418060146](https://doi.org/10.1134/S0036024418060146).
- [31] R. Louboutin, and D. Louër, Méthode directed correction des profils de raies de diffraction des rayons X. III. Sur la recherche de la solution optimale lors de la deconvolution, *Acta Cryst. A* **28** (5), 396 (1972). DOI: [10.1107/S056773947200107X](https://doi.org/10.1107/S056773947200107X).
- [32] A. L. Bail, and D. Louër, Smoothing and validity of crystallite-size distributions from X-ray line-profile analysis, *J. Appl. Crystallogr.* **11** (1), 50 (1978). DOI: [10.1107/S0021889878012662](https://doi.org/10.1107/S0021889878012662).
- [33] V. V. Zhurov, and S. A. Ivanov, PROFIT computer program for processing powder diffraction data on an IBM PC with a graphic user interface, *Crystallogr. Rep.* **42**, 202 (1997).
- [34] P. Maltoni *et al.*, Towards bi-magnetic nanocomposites as permanent magnets through the optimization of the synthesis and magnetic properties of SrFe₁₂O₁₉ nanocrystallites, *J. Phys. D: Appl. Phys.* **54** (12), 124004 (2021). DOI: [10.1088/1361-6463/abd20d](https://doi.org/10.1088/1361-6463/abd20d).
- [35] W. Kleemann, Random-field induced antiferromagnetic, ferroelectric and structural domain states, *Int. J. Mod. Phys. B* **07** (13), 2469 (1993). DOI: [10.1142/S0217979293002912](https://doi.org/10.1142/S0217979293002912).
- [36] W. Cao *et al.*, Large strain under low electric field in NBT-KBT-BT ceramics synthesized by sol-gel approach, *J. Mater. Sci.: Mater. Electron* **32**, 9500 (2021). DOI: [10.1007/s10854-021-05613-2](https://doi.org/10.1007/s10854-021-05613-2).